SODA3: a new ocean climate reanalysis

James A. Carton[1], Gennady A. Chepurin[1], and Ligang Chen[1]

To be submitted to: Monthly Weather Review

March 5, 2018

Corresponding Author: James A. Carton (carton@atmos.umd.edu)
[1]Department of Atmospheric and Oceanic Science
University of Maryland
College Park, MD 02742

Abstract

This paper describes version 3 of the Simple Ocean Data Assimilation (SODA) ocean reanalysis with enhancements to model resolution, observation and forcing data sets, and the addition of active sea ice. SODA3 relies on the ocean component of the NOAA Geophysical Fluid Dynamics CM2.5 coupled model with nominal 1/4° resolution. A scheme has also been implemented to reduce bias in the surface fluxes. A 37 year long ocean reanalysis experiment created using this new SODA3 system is compared to the previous generation of SODA (SODA2.2.4) as well as to the Hadley Center EN4.1.1 no model statistical objective analysis. The comparison is carried out in the tropics, midlatitude, and the Arctic and includes examinations of the meridional overturning circulation in the Atlantic. The comparison shows that SODA3 has reduced systematic errors to a level comparable to those of the no model statistical objective analysis in the upper ocean. The accuracy of variability has been improved poleward of the tropics, with the greatest improvements seen in the Arctic, accompanying a substantial reduction in surface net heat and freshwater flux bias. These improvements justify greater use of ocean reanalysis for climate studies including the higher latitudes.

Keywords

Data assimilation; ocean climate; reanalysis, heat flux, freshwater flux, ocean warming, sea ice

1. Introduction

Here we report on revisions to the Simple Ocean Data Assimilation (SODA) ocean reanalysis in the decade since the publication of the most recent version 2 (Carton and Giese, 2008). These revisions include changes to the ocean model, the addition of active sea ice, new forcing data sets, changes to the updating data, and modifications to the data assimilation scheme.

The origins of ocean reanalysis can be traced to efforts by meteorologists in the 1990s to use data assimilation to create uniformly gridded reconstructions of the evolving state of the global atmosphere at timescales ranging from diurnal through decadal (Kalnay et al. 1996). These atmospheric reanalyses provided, as a byproduct, all of the terms required to specify surface heat, mass, and momentum fluxes, which the oceanographers could then use to drive ocean general circulation models (e.g. Carton et al. 2000a,b). Version 2 of SODA was developed as part of an effort to address inadequacies in the initial ocean reanalyses, including ocean models that were not truly global with resolution that did not permit eddies. Several different forcing data sets were used, but for the recent version of SODA2, SODA2.2.4, forcing is provided by the NOAA 20th century reanalysis v2 (CR20v2) of Compo et al. (2011) (see Giese and Ray 2011). The data assimilation algorithm used in SODA2 was based on the computationally efficient optimal interpolation.

The design of SODA3 recognizes that future reanalyses are likely to be carried out in a fully coupled framework. For this reason SODA3 is built on the Modular Ocean Model v5 ocean component of the Geophysical Fluid Dynamics Laboratory CM2.5 coupled model (Delworth et al. 2012) with fully interactive sea ice and improved 0.25°x0.25°x50 level resolution. The

updating data sets have also been upgraded to include the latest release of the World Ocean Database, a 40% increase over the data set used in SODA2.2.4, as well as upgrades to the SST data sets. For the experiment shown here, SODA3.4.2, forcing is provided by a modified version of the European Centers for Medium Range Weather Forecasts European Reanalysis (ERA) Interim (Dee et al. 2011).

Earlier generations of ocean reanalysis have contained systematic errors which limited their usefulness for some problems such as climate change studies (for example they are not included in the Intergovernmental Panel on Climate Change fifth assessment report of Rhein et al. 2013). These systematic errors have several sources including biased observations, inaccurate model physics and numerical resolution, and biases in fluxes and initial conditions. In recent years the oceanographic community has made great efforts to remove biases from the observation sets (e.g. Levitus 2009; Boyer et al. 2016), and upgrade models to reduce model error (Balmaseda et al. 2015), leaving bias in surface fluxes (Brunke et al. 2011; Ren et al. 2014) as a major source of systematic error. In SODA3 we adopt the iterative approach of Carton et al. (2018) to address flux bias, which relies on examining the analysis increments from an initial ocean reanalysis to provide corrected fluxes for a revised ocean reanalysis. This procedure can be viewed as a step in the direction reducing systematic error in the coupled reanalysis.

Following a presentation of data and methods, Section 3 compares a new 37 year long SODA3.4.2 ocean reanalysis side by side with the previous SODA2.2.4 to available temperature and salinity data. The purpose of this comparison is to explore the issue of systematic error as well as to evaluate accuracy. We include in many of these comparisons the Hadley Center

EN4.1.1 analysis of Good et al. (2013) to clarify the changes in systematic error and accuracy that occur when shifting from a no-model statistical objective analysis to a full model-based ocean reanalysis.

2. Data and methods

This section describes the data, model, forcing, and data assimilation used in the construction and evaluation of SODA3.

2.1 Data

The main data sets that SODA ingests are the World Ocean Database of historical hydrographic profiles (Boyer et al. 2013), and in-situ and remotely sensed SST. Because of data rescue efforts the World Ocean Database now includes 15.4 million profiles. Of these, 10.8 million profiles were collected during our period of interest, including 1.8 million profiling float profiles. Between 1980 and 2000, after spatial and temporal binning, the data set contains typically 1,000-5,000 independent profiles per month, a number which increases to in excess of 10,000 profiles per month by 2010 (**Fig. 1**). Throughout this study we provide salinity values in practical salinity units based on the practical salinity scale 1978 and potential, rather than in situ, temperature.

The record prior to the 2000s is dominated by bathythermograph profiles which are subject to important evolving instrument-dependent biases (e.g. Reverdin et al. 2009). Here we adopt the corrections proposed by Levitus et al. (2009). The random error associated with the bathythermographs is also significant, but still less than the error associated with unresolved

129 processes such as tides and eddies (Janjic et al. 2017). The bathythermographs have several
130 additional limitations. First, they lack salinity observations. Second, they were shallow,
131 generally less than 700m. Third, they were mainly collected along ship tracks in the Northern
132 Hemisphere. All of these limitations have been addressed by the gradual deployment of the
133 ARGO profiling floats beginning in the early 2000s.
134
135 In addition to profile hydrography data we assimilate both in situ and satellite SST observations.
136 In situ SST observations are obtained from the International Comprehensive Ocean-Atmosphere
137 Data Set (ICOADS) version 5 release 2 SST data base (Woodruff et al. 2011). Since 1981 we
138 have also included satellite SST observations. For the period October, 1981- December, 2002
139 we use the L3 Pathfinder V5.2 Advanced Very High Resolution Radiometer SST data (Casey et
140 al. 2010). The L3 designation indicates that the product has been binned into 4 km bins, but bins
141 with no observations are unfilled. We limit the SST data we use to nighttime only to avoid
142 introducing a warm bias associated with what for our model would be an unresolved near-surface
143 diurnal warming.
144
145 The Pathfinder SST data has not been corrected for the reduction in temperature when moving
146 from the nearsurface skin layer, whose thickness is measured in microns, down to the depth of
147 the uppermost model level (*Supplemental Material,* **Fig. S1**). For SODA3 we have added an
148 empirical correction for this skin-bulk difference, following Grodsky et al. (2008). Beginning in
149 2003 we have found that Pathfinder SST has some unphysical features, including a temperature
150 spike in 2004 and a cooling trend (*Supplemental Material,* **Fig. S1**). To avoid these problems we

151 switch to the NOAA Advanced Clear Sky Processor for Ocean VIIRS and MODIS L2P
152 (ACSPO) SST product at the beginning of 2003 (Ignatov et al. 2016).
153
154 Opportunities to make a completely independent assessment of the accuracy of the ocean
155 reanalyses are limited because so much of the historical observation archive has already been
156 assimilated. Here we track forecast error by collecting statistics of the differences between the
157 assimilated observations ω^o and the forecasts of the same variables mapped onto the observation
158 locations and times: $\mathbf{H}(\omega^f)$. We track analysis error by examining the differences between ω^o
159 and the similarly mapped analysis variables $\mathbf{H}(\omega^a)$. In these expressions ω represents either
160 potential temperature or practical salinity.
161
162 As mentioned in the *Introduction* a goal of SODA3 is to reduce systematic error. To help
163 identify the presence of systematic error in SST we also compare the ocean reanalyses to the
164 1/4°x1/4° gridded objective analysis of bulk SST of Reynolds et al. (2007) and to the 1°x1°
165 gridded Meteorological Office Hadley Centre EN4.1.1 monthly subsurface temperature and
166 salinity objective analysis of Good et al. (2013). EN4.1.1 relies on the same World Ocean
167 Database 2009 data set as SODA2.2.4 with the same Levitus (2009) bathythermograph bias
168 correction as used in SODA.
169
170 SODA3 does not assimilate velocity information, which provides the opportunity to carry out an
171 independent check of ocean reanalysis velocity against Tropical Atmosphere-Ocean (TAO)
172 Triton mooring observations along the equator where the flow is ageostrophic. In the
173 subtropical North Atlantic the RAPID/AMOC measurements of overturning at 26°N provides

another opportunity to evaluate ocean reanalysis transport (Cunningham et al. 2007). This latter calculation is highly sensitive to small errors which requires that it is carried out on the original grid, which is not available for SODA2.2.4.

The cryospheric component of SODA3 is also unconstrained in the experiments described in this paper. Our examination of the cryospheric component focusses on the Arctic. In the Arctic the summer minimum sea ice extent, defined by the area of the Arctic with at least 15% sea ice concentration, varies widely from year to year. To provide some information about how well SODA3.4.2 reproduces sea ice cover we include comparison to the microwave-based concentration estimates of the seasonal minimum provided by the National Snow and Ice Data Center (NSIDC). To evaluate the mean stratification we compare the ocean reanalyses to the 1°x1° Polar science center Hydrographic Climatology version 3 (PHC3.0, Steele et al. 2001), bearing in mind that this climatology was constructed primarily from data prior to the 1990s and thus lacks the influence of the more recent Arctic warming.

2.2 Model

The global ocean/sea ice model is the ocean/sea ice component of the GFDM CM2.5 coupled model (Delworth et al. 2012) with 1440x1070 eddy permitting quasi-isotropic horizontal grid cells that vary in size from 28 km at the equator to 14 km at 60^{o}N. In the Arctic the grid splits into two geographically displaced north poles giving, for example, approximately 5 km horizontal resolution at Fram Strait east of northern Greenland. Bottom topography is based on the NOAA National Centers for Earth Information earth topography five minute grid (ETOPO5) topography (**Fig. 2**) with a few modifications to narrow passages. The topographic mask has a

number of changes from that used for SODA2 including resolved marginal seas such as Hudson Bay, and improved resolution of important passages. In the Indonesian through-flow this improved resolution allows representation of features such as Timor Strait, and Micronesia which are largely missing from the SODA2 topography (*Supplemental Material* **Fig. S2**). ETOPO5 predates much of the altimeter era and as a consequence there are a few errors in the topography, for example on the Siberian shelves.

The model has 50 levels in the vertical using a z* vertical coordinate. In the vertical the grid telescopes from 10 m resolution in the upper 100m to much coarser resolution in the deep ocean. The model uses a third order advection scheme on an Arakawa B-grid with no explicit horizontal diffusion and a scale-selective Smagorinsky viscosity, enhanced in the region of the western boundary currents. In addition, enhanced nearshore tidal mixing is parameterized. The sea ice model uses the GFDL Sea Ice Simulator dynamics and thermodynamics of Winton (2000) on the same numerical grid. Snow albedo is fixed to be 0.85, which lies in the middle of observational estimates, while ice albedo has a high value of 0.8. Surface fluxes are calculated in the GFDL Flexible Modelling System coupler, which takes into account the changing distributions of snow and ice as well as changing SST and surface currents. Monthly continental discharge is provided by Dai et al. (2009) with monthly Greenland discharge following Bamber et al. (2012).

2.3 Data Assimilation

SODA3.4.2 uses a linear deterministic sequential filter in which the ocean state ω^a is constructed from a forecast ω^f based on the difference between observations ω^o and ω^f mapped onto the observation variable and its location $\mathbf{H}(\omega^f)$:

$$\omega^a = \omega^f + \mathbf{K}[\omega^o - \mathbf{H}(\omega^f)] \tag{1.1}$$

where the gain matrix **K** determines the impact of the observations, depends on the observation error covariance $\mathbf{R}^o \equiv \left\langle \boldsymbol{\varepsilon}^o \boldsymbol{\varepsilon}^{oT} \right\rangle$ and the model forecast error covariance $\mathbf{P^f} \equiv \left\langle \boldsymbol{\varepsilon}^f \boldsymbol{\varepsilon}^{fT} \right\rangle$. A direct implementation of (1.1) would introduce shocks and spurious waves. Instead we implement the incremental analysis update procedure of Bloom et al. (1996) using an update cycle of 10 days (a period chosen to be consistent with the data sampling and the timescale of ocean variability). The form of $\mathbf{K} = \mathbf{P}^f \mathbf{H}^T \left(\mathbf{H} \mathbf{P}^f \mathbf{H}^T + \mathbf{R}^o \right)^{-1}$ is determined by minimizing the expected variance of the analysis error subject to some simplifying assumptions, including the assumption that the model forecast and observation errors are unbiased, and thus the analysis errors are unbiased. The observation errors are assumed uncorrelated (except for sea level, which is not considered here) so $\mathbf{R}^o$ is diagonal.

$\mathbf{R}^o$ has been diagonalized due to the assumption that observation error is uncorrelated white noise. For the experiment described here the model forecast error P^f has the form

$$\mathbf{P^f}(\Delta x, \Delta y, \Delta z, \Delta t, \bar{y}, z_1, z_2, \rho(z), \Delta\eta) = \Phi\, e^{-\left[\frac{\Delta\eta^2}{\gamma_\eta^2} + \left| \frac{\Delta x}{\gamma_x} \right| + \left| \frac{\Delta y}{\gamma_y} \right| + \left| \frac{\Delta z}{\gamma_z} \right| + \left| \frac{\Delta t}{\gamma_t} \right| \right]} \tag{1.2}$$

with pre-specified dependence on the zonal (Δx), meridional (Δy), and vertical (Δz) spatial and time (Δt) difference between forecast and observation points. The dependence of $\mathbf{P}^f$ on change

241 in sea level height $\Delta\eta$ with $\gamma_\eta = 1m$ allows the error covariance to depend on the flow field,
242 elongating the error covariance scale along strong currents such as the Gulf Stream. For the
243 other scales (γ_i) we follow Carton and Giese (2008) who include some anisotropy (zonal scales
244 are larger than meridional scales in the tropics) and some latitude dependence (horizontal scales
245 decrease somewhat with increasing latitude). Experiments have shown a general lack of
246 sensitivity of the ocean reanalysis to the specification of these scales. A significant improvement
247 can be obtained by switching to replacing (1.2) with an evolving estimate from an ensemble
248 Kalman Filter (Penny et al. 2015), but will increase the computational cost by perhaps a factor of
249 50.
250
251 The forecast error covariance between temperature and salinity errors is determined from an
252 empirical table constructed from the hydrographic profile data set. The intention is to maintain
253 water mass properties if only one of those variables (generally temperature) is assimilated.
254 **Figure 3** illustrates the relationship between these variables at a single location in the western
255 subtropical North Atlantic. At this location the temperature-salinity relationship is quite similar
256 for all three analyses we consider, SODA3.4.2, SODA2.2.4, and EN4.1.1 at levels shallower than
257 about 900m. At deeper levels, the SODA2.2.4 temperature-salinity relationship has greater
258 scatter indicating that new water masses are being created.
259
260 The oceanic mixed layer is special because of the well-mixed properties and because of the high
261 observational sampling. In SODA3 we estimate the mixed layer depth each assimilation cycle
262 from the forecast using the 0.125 σ – based criterion of Kara et al. (2003). The analysis of mixed
263 layer properties is made first at 5m depth and then is propagated down through the mixed layer.

264

265 *2.4 Surface forcing*

266 SODA3.4.2 is forced by ERA-Interim (Dee et al. 2011) six-hourly near-surface atmospheric
267 variables (U_{10m}, Ta_{2m}, q_{2m}, sea level pressure, and precipitation) together with downwelling short
268 and longwave radiative fluxes. These are applied to the ocean-sea ice system through the GFDL
269 Flexible Model System flux coupler and either one of two sets of bulk flux formulas: the
270 Coupled Ocean-Atmosphere Response Experiment (Fairall et al. 2003) version 4 (COARE4).
271 We evaluate the compatibility of this flux specification by accumulating the gridded potential
272 temperature and salinity analysis increments ($\delta\theta = \mathbf{K}[\theta^o - \mathbf{H}(\theta^f)]$ and $\delta S = \mathbf{K}[S^o - \mathbf{H}(S^f)]$)
273 during a preliminary eight year ocean reanalysis 2007-2014. A latitudinal slice of the time mean
274 of these increments is shown in **Fig. 4** (upper panels)**.** It is evident that the increments are largest
275 within the mixed layer except where the currents are strong. As explored in Carton et al (2018),
276 these time mean increments reflect the presence of biases in net surface heat and freshwater flux.
277 We can estimate the required modifications to net surface heat, δQ, and freshwater flux,
278 $\delta(P-E+R)$, from the incremental heat and freshwater budgets:

279

280
$$\delta Q \approx \frac{\rho C_p}{\Delta t} \int_{z=-D}^{0} \delta\theta dz$$
$$\delta(P-E+R) \approx \frac{1}{S_o \Delta t} \int_{z=-D}^{0} \delta S dz \qquad (1.3)$$

281

282 Where D is the depth of the mixed layer, S_o is surface salinity, ρ is water density, C_p is water
283 specific heat, and $\Delta t = 10dy$ is the length of an assimilation cycle. *Supplemental Material* **Fig.**
284 **S3** shows the geographic structure of the resulting modifications to time mean ERA-Interim heat

and freshwater fluxes while the modified fluxes are shown in **Fig. 5**. To illustrate the impact of the flux bias-correction procedure we present the time mean analysis increments of potential temperature and salinity SODA3.4.2 (which uses the modified fluxes) in the lower panels of **Fig. 4.** Modifying the fluxes reduces the analysis increments and thus increases the compatibility of heat and freshwater exchanges between atmosphere and ocean.

2.5 Output data sets

Ocean reanalysis output is saved separately for the ocean and sea ice variables on the native grid at 5dy resolution. The ocean files contain the ocean state (temperature, salinity, and velocity) as well as a number of diagnostic variables such as mixed layer depth and entrainment, individual components of net surface heat flux, sea level, etc. Volume transport estimates in and out of each model cell are saved on the original grid in a separate file at 10dy resolution.

A subset of the variables contained in the original files are regridded onto a uniform 0.5°x0.5° horizontal grid using a conservative mapping scheme (retaining the original vertical grid), and then are also monthly averaged (both 5dy and monthly average regridded datasets are available). A one year long file containing 12 monthly regridded ocean datasets is 3.3Gb, while the corresponding regridded file containing sea ice variables (thickness categories and concentration) is 88Mb. Finally, some ancillary fields are created from the regridded files. These include depth, potential temperature, and salinity on 16 iso-potential density surfaces ranging from 1028 kg m^{-3} to 1024 kg m^{-3}.

3. Results

We begin by comparing potential temperature and salinity fields at 5m depth on monthly timescales during 1980-2008, using the gridded OISST analysis of Reynolds et al (2007) for this comparison (**Fig. 6**). The time mean differences show that both SODA3.4.2 and SODA2.2.4 have a small 0.25°C warmer bulk mixed layer than OISST throughout much of the northern subtropics. As shown in *Supplemental Material,* **Fig. S1** a difference of this size can be introduced simply by the choice of observation sets. In contrast, south of 60°S SODA2.2.4 has a 1°C warm bias which we think is due to the lack of sea ice. SODA2.2.4 monthly variability is synchronized with OISST only in the tropics (**Fig. 6** righthand panels). At higher latitudes the two vary independently at monthly timescales.

3.1 Upper and mid-depth layers

We next examine subsurface potential temperature and salinity beginning with the upper 300m. For this comparison we map the ocean reanalyses onto the hydrographic profile observation locations, compute the analysis increments ($\mathbf{H}(\omega^a) - \omega^o$), and then accumulate the time average statistics (mean and root mean square). The mean of the analysis increments reveals that EN4.1.1 is nearly unbiased, SODA3.4.2 has a warm bias confined to the Pacific and Atlantic equator, while SODA2.2.4 is systematically cool and generally fresh (**Figs. 7** and **8** lefthand panels). The cause of the SODA3.4.2 equatorial warm bias has been traced to the strength of the ERA-Interim equatorial trade winds which are slightly weak (Dussin et al. 2016), thus providing insufficient equatorial upwelling. The root mean square of the analysis minus observation misfits (**Figs. 7** and **8** righthand panels) shows that outside of the tropics the SODA2.2.4 analysis errors are within a factor of two of the monthly variability. In contrast both

330 SODA3.4.2 and EN4.1.1 show lower RMS differences between the analyses and the observation
331 set in the 0-300m layer.
332
333 One component of the 0-300m monthly potential temperature variability is a weak 0.008 K/yr
334 (equivalent to a quarter of a W/m^2) global warming trend, which represents part of the ocean's
335 uptake of the global heat flux imbalance introduced by changing greenhouse gas levels in the
336 atmosphere. All three analyses show quite similar vertically averaged temperature trends, as
337 well as similar details such as the cooling of the upper ocean in the early 1980s and again
338 following the 1991 eruption of Mount Pinatubo (**Fig. 9** lefthand panels). None of the analyses
339 show much indication of the widely-discussed heat storage hiatus of the early 2000's. The 300–
340 1000m layer warms at an average rate 1/4 that of the upper 300m (and thus storing 60% as much
341 of the excess planetary heat as the upper layer). In the 1000m-2000m layer EN4.1.1 and
342 SODA3.4.2 are also warming however we do not know the extent to which the increase with
343 time of the observation count in this depth range may contribute to this result.
344
345 Global average salinity is nearly constant due to the lack of salt sources. However, shifts in the
346 strength of the atmospheric hydrologic cycle seem to cause basin-scale changes in sea surface
347 salinity (Durack and Wijffels 2010). A recent study by Friedman et al. (2017) suggests that the
348 most dramatic change in recent decades has been the salinification of the surface Atlantic 40°S-
349 40°N, a result which motivates our examination of Atlantic salinity (**Fig. 9** righthand panels).
350 While quite noisy, all three analyses do show increasing 0-300m salinity during 1980-2008.
351 However, as with 1000m-2000m temperatures, we do not know the extent to which the observed

positive subsurface salinity trend is caused by the increasing salinity observation count after year 2000.

Closely tied to the issue of changing Atlantic salinity is the issue of the changing strength of the meridional overturning circulation. In a previous study using SODA2 Zheng and Giese (2009) estimate a mean overturning transport a 26°N of approximately $16x10^6$ m^3/s and also document indications of an increasing transport trend over multiple decades. Since 2004 direct observations have been collected by the RAPID/AMOC array at this latitude (Cunningham et al. 2007) which can now be directly compared to SODA3.4.2 monthly transport estimates (**Fig. 10).** The comparison shows a remarkably close correspondence at seasonal timescales, with similar year-to-year variations and indications of a decline in transport by $1\text{-}2x10^6$ m^3/s since 2004.

3.2 Arctic

The Arctic is a salinity-controlled, highly stratified ocean, with a cold and fresh shallow surface layer overlying a warmer, saltier upper layer. On the Atlantic side of the Arctic this warm/salty layer is supplied by Atlantic Water flowing northward through Fram Strait and eastward across the Barents Sea Opening. On the Pacific side of the Arctic somewhat cooler, fresher Pacific Water flows north through Bering Strait and eastward into the Canada basin. In **Fig. 11** we examine the time mean stratification at two locations on opposite sides of the Arctic that sample these water masses.

On the Atlantic side, in the Nansen basin northeast of Svalbard, observations (Anderson and Jones, 1992) and the PHC3.0 climatology both show a pronounced warm >1°C, salty >34.6psu,

375 Atlantic Water layer at depths between 200m and 500m (**Fig. 11** upper panels). SODA3.4.2 has
376 similar salinity stratification, but with Atlantic Water temperatures that are up to 0.5°C warmer
377 than the PHC3.0 climatology, perhaps reflecting the impact of the recent warming of this water
378 mass (Polyakov et al. 2005; Beszczynska-Möller et al. 2012). In SODA2.2.4, in contrast, the
379 Atlantic Water layer rises close to the surface layer. The surface layer in PHC3.0 and
380 SODA3.4.2 is low salinity (33 psu) and near-freezing, consistent with the presence of sea ice.
381 SODA2.2.4, in contrast, has an erroneously warm (0°C) surface layer, much as it does in the
382 Antarctic as well (**Fig. 6**).
383
384 On the Pacific side of the Arctic, east of Bering Strait and within the Beaufort Gyre, PHC3.0 and
385 SODA3.4.2 (**Fig. 11** lower panels) have a deeper and cooler halocline that freshens to <30 psu at
386 the surface. PHC3.0 also has a thermostad of cool <-1°C water of Pacific origin lying between
387 50 and 200m which is absent from SODA3.4.2 despite the fact that this reanalysis has reasonable
388 1.1×10^6 m^3/s transport through Bering Strait. Observational studies show the upper 50 m has
389 complex properties (Shimada et al. 2001; Shimada et al. 2005). Sub-zero surface temperatures
390 are separated from the thermostad by a thin shallow temperature maximum, the existence of
391 which is indicated by a slight temperature peak in PHC3.0 at 75m depth. This shallow
392 temperature maximum is missing from SODA3.4.2. SODA2.2.4 has nearsufarce properties that
393 differ from PHC3.0 and SODA3.4.2, being both very fresh and warming dramatically towards
394 the surface.
395
396 *3.2.1 Sea ice* We evaluate the performance of the SODA3.4.2 sea ice by comparing the seasonal
397 minimum sea ice extent to the observed record whose most dramatic observed feature is the

gradual decline in seasonal minimum extent. The observations and SODA3.4.2 both show a gradual 0.7%/yr decline in extent, along with similar year-to-year variability **(Fig. 12**). Studies of the causes of the two summers of extreme sea ice loss, 2007 and 2012, highlight the importance of anomalous solar insolation and wind-driven sea ice export from the Arctic (Parkinson and Comiso 2013). The appearance of these features in SODA3.4.2 may suggest that these processes are being handled correctly. Alternatively the good agreement in **Fig. 12** could be due partly to the imprint of the observed sea ice extent on the distribution of SST observations (no observations where there is sea ice) and surface flux forcing (surface air temperature and air humidity are lower over sea ice).

3.3 Tropics

Finally we consider the behavior of the ocean reanalyses along the equator, focusing on the Pacific sector. The good agreement with observed temperature and salinity evident in **Figs. 7** and **8** is confirmed in a comparison to the time mean profiles of temperature and salinity at two mooring locations in the central-western (165°E) and eastern (140°W) Equatorial Pacific (**Fig. 13**). The central-western Pacific has a rain-freshened surface layer which is slightly fresher than in the ocean reanalyses. From 165°E to 140°W the observed depth of the peak speed of the observed eastward Equatorial Undercurrent shallows from 200m to 110m and that peak speed strengthens to > 1 m/s. Both SODA3.4.2 and SODA2.2.4 have Equatorial Undercurrents that are too weak and shallow at 165°E, while they strengthen to match the observations by 140°W.

In the central/western basin the observations and SODA3.4.2 both have surface currents that vary in response to changing meteorological conditions such as those associated with El Nino,

but have a weak time mean. A striking feature of the 1997/8 El Nino, for example, is the appearance of multiple westerly wind bursts in the first half of 1997 (van Oldenborgh 2000), driving eastward surface currents in the central basin that persist for much of 1997. Such strong eastward currents are evident in SODA3.4.2 throughout 1997, but are confined to the boreal spring season in SODA2.2.4 (**Fig. 14**).

4. Summary and Discussion

This article describes construction of version 3 of the Simple Ocean Data Assimilation (SODA) ocean reanalysis, which follows the previous update of SODA (Carton and Giese 2008) a decade ago. SODA3 is built around the eddy-permitting Modular Ocean Model v5 component of the GFDL CM2.5 coupled model and includes SIS interactive sea ice at high latitudes. Other changes include updates to the data sets being assimilated and changes to the surface forcing fields. Attention is focused on reducing systematic errors by reducing biases in surface heat and freshwater fluxes. For the experiment described here the data assimilation is a simple but efficient implementation of optimal interpolation with modifications to account for mixed layer dynamics. Implementation of an ensemble Kalman Filter is described separately in Penny et al. (2015).

To evaluate the performance of SODA3 we compare a 37 year long ocean reanalysis experiment (SODA3.4.2) forced by ERA-Interim forcing modified to reduce bias, to a version of the earlier SODA2 (SODA2.2.4) and to the no-model EN4.1.1 statistical objective analysis during their 28 year period of overlap 1980-2008. We begin by comparing the two ocean reanalyses to the Reynolds et al. (2007) OISSTv2 statistical objective analysis of nominally bulk SST. This

444 comparison reveals that SODA2.2.4 SST is too cool and has a noise level, determined by the
445 RMS difference from OISSTv2, of 0.6 to 1°C. In contrast, for EN4.1.1 and SODA3.4.2 the only
446 systematic difference from OISSTv2 is an equatorial upwelling-related warm bias in the Atlantic
447 and Pacific in SODA3.4.2. EN4.1.1 and SODA3.4.2 have SST noise levels of less than 0.6°C.
448
449 We next examine monthly temperature and salinity in the 0/300m layer in comparison to the
450 historical hydrographic profile data set (**Figs. 7** and **8**). Again, SODA2.2.4 is systematically
451 cooler than the observations with a 0/300m temperature noise level of 0.1°C (**Fig. 7**). EN4.1.1
452 and SODA3.4.2 have little indication of systematic error and low noise levels. All three analyses
453 show a similar rate of warming of the upper 1000m of approximately 0.4 W/m^2, interrupted by 1-
454 2 cool years following the 1991 eruption of Mount Pinatubo (**Fig. 9** lefthand panels). They show
455 little evidence of a hiatus in the rate of ocean warming that has been suggested as having
456 occurred in the early 2000's.
457
458 SODA2.2.4 0/300m monthly salinity is systematically low in the tropics and subtropics while the
459 other two analyses have less evidence of systematic error and lower noise levels (**Fig. 8**). All
460 three analyses show that the upper layers of the Atlantic, 40°S-40°N are becoming more saline.
461 However, the timing of this salinification also corresponds to the introduction of the Argo
462 salinity observations in the early 2000's raising concerns that the apparent increase in salinity
463 reflects the changing observing system. Finally, we show an encouragingly close
464 correspondence between the SODA3.4.2 overturning circulation and the decade-long observed
465 record at 26°N in the Atlantic.
466

In the Arctic we compare the stratification at two locations on either side of the Arctic to the PHC3.0 climatology. The correspondence between PHC3.0 and SODA3.4.2 is generally good with two exceptions. SODA3.4.2 has 0.5-1K warmer temperatures for the layers containing water of Atlantic and Pacific origin than PHC3.0 (possibly reflecting the warming of these layers in recent years). SODA2.2.4 shows more dramatic differences, including vertical displacements of water masses and excess freshening of the Pacific side of the Arctic. The lack of sea ice in SODA2.2.4 seems to lead to excess heating of the surface layer, raising SST by as much as 2K. In contrast, the SODA3.4.2 sea ice extent compares well with the observed record. Finally, we examine the behavior of the reanalyses in the tropics. In the tropics SODA3.4.2 and SODA2.2.4 are similar and both are consistent with observations. The main differences we've identified are the near-surface velocity fields which may reflect differences in specified surface momentum fluxes.

While we still need to clarify the errors introduced into the ocean reanalysis by the remaining surface flux errors, the changing ocean observing system, model numerics, and limitations of the data assimilation schemes, we believe the improvements to SODA support greater use for climate studies particularly involving the higher latitudes.

Acknowledgments and Data links Computing resources were provided by the Computational and Information Systems Laboratory of NCAR. The complete hydrographic data set was obtained from the NOAA National Center for Environmental Information World Ocean Database (www.nodc.noaa.gov). In situ SST observations were obtained from the ICOADS archive which is hosted by the U.S. National Oceanic and Atmospheric Administration (icoads.noaa.gov/e-doc). Satellite AVHRR Pathfinder Version 5.2 (PFV5.2) SSTs were obtained from the US National Oceanographic Data Center and GHRSST (pathfinder.nodc.noaa.gov). PFV5.2 is an updated version of the Pathfinder Version 5.0 and 5.1 collection described in Casey et al. (2010). ACSPO MODIS SST data are provided by NOAA STAR. We strongly recommend contacting NOAA SST team led by A. Ignatov before the data are used for any publication or presentation. EN4.1.1 is a product of the UK Met. Office Hadley center, [September, 2017]. The Polar science center Hydrographic Climatology (PHC) PHC3.0 climatology was obtained from the Applied Physics Laboratory (psc.apl.washington.edu/nonwp_projects/PHC/Data3.html). The National Snow and Ice Data Center (NSIDC) Arctic sea ice extent was calculated from the updated daily sea ice extent Version 2.1 [September, 2017]. The Tao triton time series were obtained from the NOAA Ocean Climate Stations Project Office of the NOAA/PMEL (www.pmel.noaa.gov/tao/drupal/disdel/), [September, 2017]. RAPID/AMOC Data from the RAPID-WATCH MOC monitoring project are funded by the Natural Environment Research Council and and were obtained from www.rapid.ac.uk/rapidmoc [January, 2016]. doi for this data set is: 10.5285/5acfd143-1104-7b58-e053-6c86abc0d94b. Most of all, we are grateful to Eric Itsweire and the Physical Oceanography Program of the National Science Foundation (OCE1233942) for providing financial support for this work. The SODA3.4.2 reanalysis data sets are available through www.soda.umd.edu.

509 **References**

510 Anderson, L.G., and E.P. Jones (1992), Tracing upper waters of the Nansen Basin in the Arctic
511 Ocean, *Deep-Sea Res*., Part A, **39**, suppl. 2, S425-S433,.

512 Balmaseda, MA F. Hernandez, A. Storto, et al. (2015), The Ocean Reanalyses Intercomparison
513 Project (ORA-IP), *J. Operational Oceanography*, **8**, S80-S97, DOI:
514 10.1080/1755876X.2015.1022329

515 Bamber, J., M. vanden Broeke, J. Ettema, J. Lenaerts, and E. Rignot (2012), Recent large
516 increases in freshwater fluxes from Greenland into the North Atlantic, *Geophys. Res.*
517 *Letts.*, **39**, L19501, doi:10.1029/2012GL052552.

518 Beszczynska-Möller, A., E. Fahrbach, U. Schauer, and E. Hansen (2012), Variability in Atlantic
519 water temperature and transport at the entrance to the Arctic Ocean, 1997–2010, *ICES J.*
520 *Mar. Sci.*, **69**, 852–863.

521 Bloom, S.C., L.L. Takacs, A.M. da Silva, and D. Ledvina (1996), Data Assimilation Using
522 Incremental Analysis Updates. *Mon. Wea. Rev*., **124**, 1256–1271,
523 https://doi.org/10.1175/1520-0493(1996)124<1256:DAUIAU>2.0.CO;2

524 Boyer, T.P., J.I. Antonov, O.K. Baranova, C. Coleman, H.E. Garcia, A. Grodsky, D.R. Johnson,
525 R.A. Locarnini, A.V. Mishonov, T.D. O'Brien, C.R. Paver, J.R. Reagan, D. Seidov, I. V.
526 Smolyar, and M. M. Zweng (2013), World Ocean Database 2013, NOAA Atlas NESDIS
527 72, S. Levitus, Ed., A. Mishonov, Technical Ed.; Silver Spring, MD, 209 pp.

528 Boyer, T.P., et al. (2016), Sensitivity of global upper ocean heat content estimates to mapping
529 methods, XBT bias corrections, and baseline climatologies, *J. Clim*., **29**, 4817–4842,
530 doi:10.1175/JCLI-D-15-0801.1.

Brunke, M. A., Z. Wang, X. B. Zeng, M. Bosilovich and C. L. Shie (2011), An assessment of the uncertainties in ocean surface turbulent fluxes in 11 reanalysis, satellite-derived, and combined global datasets, *J. Clim.*, **24**, 5469-5493.

Carton, J.A., and B.S. Giese (2008), SODA: A Reanalysis of Ocean Climate, *Mon. Wea. Rev.,* **136**, 2999-3017.

Carton, J.A., G. Chepurin, X. Cao, and B.S. Giese (2000a), A Simple Ocean Data Assimilation analysis of the global upper ocean 1950-1995, Part 1: methodology, *J. Phys. Oceanogr.*, **30**, 294-309.

Carton, J.A., G. Chepurin, and X. Cao (2000b), A Simple Ocean Data Assimilation analysis of the global upper ocean 1950-1995 Part 2: results, *J. Phys. Oceanogr.*, **30**, 311-326.

Carton, J.A., G.A. Chepurin, L. Chen, and S.A. Grodsky (2018), Improved global net surface heat flux, *J. Geophysical Res.*, in press.

Casey, K.S., T.B. Brandon, P. Cornillon, and R. Evans (2010), "The Past, Present and Future of the AVHRR Pathfinder SST Program", in Oceanography from Space: Revisited, eds. V. Barale, J.F.R. Gower, and L. Alberotanza, Springer. DOI: 10.1007/978-90-481-8681-5_16.

Compo, G.P., J.S. Whitaker, P.D. Sardeschmukh, N. Matsui, R. J. Allan, X. Yin, B. E. Gleason, R. S. Vose, G. Rutledge, P. Bessemoulin, S. Brönnimann, M. Brunet, R. I. Crouthamel, A. N. Grant, P. Y. Groisman, P. D. Jones, M. C. Kruk, A. C. Kruger, G. J. Marshall, M. Maugeri, H. Y. Mok, Ø. Nordli, T. F. Ross, R. M. Trigo, X. L. Wang, S. D. Woodruff and S. J. Worley (2011), The Twentieth Century Reanalysis Project, *Q. J. Roy. Meteorol. Soc.*, **137**, 1-28. DOI: 10.1002/qj.776

553 Cunningham, S. A., T. Kanzow, D. Rayner, M.O. Baringer, W.E. Johns, J. Marotzke, H. R.
554 Longworth, E.M. Grant, J. J-M. Hirschi, L.M. Beal, C.S. Meinen, H.L. Bryden (2007),
555 Temporal variability of the Atlantic meridional overturning circulation at 26.5°N,
556 *Science*, **317**, 935-938. doi:10.1126/science.1141304
557 Dai, A., T. Qian, and K.E. Trenberth, 2009: Changes in Continental Freshwater Discharge from
558 1948 to 2004, *J. Clim.*, **22**, 2773-2792. DOI: 10.1175/2008JCLI2592.1
559 Dee, D. P., Uppala, S. M., Simmons, A. J., Berrisford, P., Poli, P., Kobayashi, S., Andrae, U.,
560 Balmaseda, M. A., Balsamo, G., Bauer, P., Bechtold, P., Beljaars, A. C. M., van de Berg,
561 L., Bidlot, J., Bormann, N., Delsol, C., Dragani, R., Fuentes, M., Geer, A. J., Haimberger,
562 L., Healy, S. B., Hersbach, H., Hólm, E. V., Isaksen, L., Kållberg, P., Köhler, M.,
563 Matricardi, M., McNally, A. P., Monge-Sanz, B. M., Morcrette, J.-J., Park, B.-K.,
564 Peubey, C., de Rosnay, P., Tavolato, C., Thépaut, J.-N. and Vitart, F. (2011), The ERA-
565 Interim reanalysis: configuration and performance of the data assimilation system. *Q.J.R.*
566 *Meteorol. Soc.*, **137**, 553–597. doi: 10.1002/qj.828
567 Delworth, T.L., A. Rosati, W. Anderson, A.J. Adcroft, V. Balaji, R. Benson, K. Dixon, S. M.
568 Griffies, H.-C. Lee, R.C. Pacanowski, G.A. Vecchi, A.T. Wittenberg, F. Zeng, and R.
569 Zhang (2012), Simulated Climate and Climate Change in the GFDL CM2.5 High-
570 Resolution Coupled Climate Model. *J. Clim.*, **25**, 2755–2781. doi:
571 http://dx.doi.org/10.1175/JCLI-D-11-00316.
572 Durack, P.J. and S.E. Wijffels, 2010: Fifty-Year Trends in Global Ocean Salinities and Their
573 Relationship to Broad-Scale Warming. *J. Climate*, **23**, 4342–4362,
574 https://doi.org/10.1175/2010JCLI3377.1

575 Dussin, R., B. Barneir, L. Brodeau, and J.M. Molines (2016), The making of the DRAKKAR
576 forcing set DFS5 DRAKKAR/MyOcean Report 01-04-16. https://www.drakkar-
577 ocean.eu/publications/reports/report_DFS5v3_April2016.pdf. Accessed August, 2017.
578 Fairall, C.W., E.F. Bradley, J.E. Hare, A.A. Grachev, and J.B. Edson (2003), Bulk
579 Parameterization of Air–Sea Fluxes: Updates and Verification for the COARE
580 Algorithm. *J. Climate*, **16**, 571–591, https://doi.org/10.1175/1520-
581 0442(2003)016<0571:BPOASF>2.0.CO;2
582 Fetterer, F., K. Knowles, W. Meier, M. Savoie, and A. K. Windnagel. 2017
583 Friedman, A.R., G. Reverdin, M. Khodri, and G. Gastineau (2017), A new record of Atlantic sea
584 surface salinity from 1896 to 2013 reveals the signatures of climate variability and long-
585 term trends. *Geophys. Res. Lett.*, **44**, 1866–1876, doi:
586 https://doi.org/10.1002/2017GL072582.
587 Giese, B.S., and S. Ray (2011), El Nino variability in simple ocean data assimilation (SODA),
588 1871-2008, *J. Geophys. Res*., **116**, Article Number: C02024
589 Good, S.A., M.J. Martin and N.A. Rayner, 2013. EN4: quality controlled ocean temperature and
590 salinity profiles and monthly objective analyses with uncertainty estimates, *J. Geophys.*
591 *Res.*, **118**, 6704-6716, doi:10.1002/2013JC009067
592 Grodsky, S.A., J.A. Carton, and H. Liu, 2008: Comparison of bulk sea surface and mixed layer
593 temperatures, *J. Geophys. Res.*, **113**, C10026, doi:10.1029/2008JC004871.
594 Ignatov, A., X. Zhou, B. Petrenko, X. Liang, Y. Kihai, P. Dash, J. Stroup, J. Sapper, and P.
595 DiGiacomo (2016), AVHRR GAC SST Reanalysis Version 1 (RAN1), *Remote Sens.*, **8**,
596 315; doi:10.3390/rs8040315

Janjić, T., N. Bormann, M. Bocquet, J.A. Carton, S.E. Cohn, S.L. Dance, S.N. Losa, N.K. Nichols, R. Potthast, R., J.A. Waller, and P. Weston (2017), On the representation error in data assimilation. *Q.J.R. Meteorol. Soc.* doi:10.1002/qj.3130

Kalnay, E., M. Kanamitsu, R. Kistler, W. Collins, D. Deaven, L. Gandin, M. Iredell, S. Saha, G. White, J. Woollen, Y. Zhu, A. Leetmaa, R. Reynolds, M. Chelliah, W. Ebisuzaki, W. Higgins, J. Janowiak, K.C. Mo, C. Ropelewski, J. Wang, R. Jenne, and D. Joseph, 1996: The NCEP/NCAR 40-Year Reanalysis Project. *Bull. Amer. Meteor. Soc.,* **77**, 437–471, https://doi.org/10.1175/1520-0477(1996)077<0437:TNYRP>2.0.CO;2

Kara, A. B., P. A. Rochford, and H. E. Hurlburt (2003), Mixed layer depth variability over the global ocean, *J. Geophys. Res*., **108**, 3079, doi:10.1029/2000JC000736, C3.

Levitus, S., J. I. Antonov, T. Boyer, R. A. Locamini, H. E. Garcia, and A. V. Mishonov (2009), Global ocean heat content 1955-2008 in light of recently revealed instrumentation problems. *Geophys. Res. Lett.*, **36**, L07608, doi:10.1029/2008GL037155.

Parkinson CL, JC Comiso (2013), On the 2012 record low Arctic sea ice cover: combined impact of preconditioning and an August storm. *Geophys Res Lett*, **40**, 1356–1361

Penny, S.G., D.W. Behringer, J.A. Carton, and E. Kalnay, 2015: A Hybrid Global Ocean Data Assimilation System at NCEP, *Mon. Wea. Rev.*, **143**, 4660-4677.

Polyakov, I. V., et al. (2005), One more step toward a warmer Arctic, *Geophys. Res. Lett.*, **32**, L17605, doi:10.1029/2005GL023740.

Ren, L., E. Hackert, P. Arkin, and A. J. Busalacchi (2014), Estimating the global oceanic net freshwater flux from Argo and comparing it with satellite-based freshwater flux products, *J. Geophys. Res*., **119**, 7869–7881, doi:10.1002/2013JC009620.

619 Reverdin, G., F. Marin, B. Bourles, and P. L'Herminier (2009), XBT temperature errors during
620 French research cruises (1999–2009). *J. Atmos. Oceanic Technol.*, **26**, 2462–2473.
621 Reynolds, R.W., T.M. Smith, C. Liu, D.B. Chelton, K.S. Casey and M.G. Schlax (2007), Daily
622 High-resolution Blended Analyses for sea surface temperature. *J. Climate*, **20**, 5473-
623 5496.
624 Rhein, M., S.R. Rintoul, S. Aoki, E. Campos, D. Chambers, R.A. Feely, S. Gulev, G.C. Johnson,
625 S.A. Josey, A. Kostianoy, C. Mauritzen, D. Roemmich, L.D. Talley and F. Wang (2013),
626 Observations: Ocean. In: Climate Change 2013: The Physical Science Basis.Contribution
627 of Working Group I to the Fifth Assessment Report of the Intergovernmental Panel on
628 Climate Change [Stocker, T.F., D. Qin, G.-K. Plattner, M. Tignor, S.K. Allen, J.
629 Boschung, A. Nauels, Y. Xia, V. Bex and P.M. Midgley (eds.)]. Cambridge University
630 Press, Cambridge, United Kingdom and New York, NY, USA
631 Shimada, K., E. C. Carmack, K. Hatakeyama, and T. Takizawa (2001), Varieties of shallow
632 temperature maximum waters in the western Canadian Basin of the Arctic Ocean,
633 *Geophys. Res. Lett.*, **28**, 3441–3444.
634 Shimada, K., M. Itoh, S. Nishino, F. McLaughlin, E. Carmack, and A. Proshutinsky (2005),
635 Halocline structure in the Canada Basin of the Arctic Ocean, *Geophys. Res. Lett*., **32**,
636 L03605, doi:10.1029/2004GL021358.
637 Steele, M., R. Morley, and W. Ermold (2001), PHC: A global ocean hydrography with a high
638 quality Arctic Ocean, *J. Climate*, **14**, 2079-2087.
639 van Oldenborgh, G.J. (2000), What Caused the Onset of the 1997–98 El Niño?, *Mon. Wea. Rev*.,
640 **128**, 2601–2607, https://doi.org/10.1175/1520-
641 0493(2000)128<2601:WCTOOT>2.0.CO;2

642 Winton, M. (2000), A reformulated three-layer sea ice model, *J. Atmos. Ocean Technol.*, **17**,
643 525–531.
644 Woodruff SD, S.J. Worley, S.J. Lubker, Z. Ji, J.E. Freeman, D.I. Berry, P. Brohan, E.C. Kent,
645 R.W. Reynolds, S.R. Smith, and C. Wilkinson (2011), ICOADS Release 2.5: Extensions
646 and enhancements to the surface marine meteorological archive, *Int. J. Climatol*., **31**,
647 951-967. DOI: 10.1002/joc.2103\
648 Zheng, Y., and B. S. Giese (2009), Ocean heat transport in Simple Ocean Data Assimilation:
649 Structure and mechanisms, *J. Geophys. Res.*, **114**, C11009, doi:10.1029/2008JC005190.
650

Figure legends

Fig. 1 **soda3_data_distrib.pdf** Number of hydrographic profile observations used by SODA3, after spatial and temporal binning to remove redundancies, with depth and time 1980-2015. Upper panel shows temperature, lower panel shows salinity. Units: observations per month.

Fig. 2 **soda3_global_topography.pdf** ETOP5 topography used in SODA3. Note the inclusion of many marginal seas. Units are m.

Fig. 3 **ts-bermuda.pdf** Potential temperature versus salinity for (green) SODA2.2.4, (red) SODA3.4.2, and (black) EN4.1.1 at a fixed location (32°N, 62°W) just east of Bermuda in the subtropical North Atlantic for the nine year period 2000-2008. The temperature/salinity relationship is reasonably consistent among the three except for temperatures below 8°C corresponding to depths below 900m. At those depths SODA2.2.4 shows greater variability. Units are K and psu.

Fig. 4 **180w_increment.pdf** Mean (left) temperature increments $\overline{\theta^o - \mathbf{H}(\theta^f)}$ and (right) salinity increments $\overline{S^o - \mathbf{H}(S^f)}$ with latitude and depth, averaged in the longitude band 170°W-180°W for experiments using ERA-Int forcing. The average depth of the density-based mixed layer is shown in black and zonal velocity in green (0.2 m/s contour). Upper panels show analysis increments before heat and freshwater fluxes are corrected. Lower panels show analysis increments for SODA3.4.2, after heat and freshwater fluxes have been corrected as described in the text. Note the reduction in misfit except near the strong equatorial currents. Units are K/10dy and psu/10dy.

Fig. 5 **flxs_soda342.pdf** Time mean net surface heat flux. Units are W/m^2 and mm/dy.

673 Fig. 6 **Fig. SST_compare_342_224.pdf** (left) Mean and (right) root mean square difference of
674 monthly SST from the OISST analysis of Reynolds et al. (2007). (upper) SODA3.4.2,
675 (lower) SODA2.2.4. Units are K.
676 Fig. 7 **A-O_temp_comparison.pdf** Statistics of the binned analysis minus observation potential
677 temperature differences $\mathbf{H}(\theta^a) - \theta^o$ averaged 0-300m during the 29 year period 1980-
678 2008. (Upper row) SODA3.4.2 - OBS, (middle row) SODA2.2.4 – OBS, (lower row)
679 EN4.1.1 – OBS. (left) Mean, (Right) RMS. Units are K. Contours of the RMS
680 variability of 0/300m temperature are superposed on upper right panel for comparison (CI
681 = 1 K).
682 Fig. 8 **Fig. A-O_salt__comparison.pdf** Statistics of the binned analysis minus observation
683 salinity differences $\mathbf{H}(S^a) - S^o$ averaged 0-300m during the 29 year period 1980-2008.
684 (Upper row) SODA3.4.2 - OBS, (middle row) SODA2.2.4 – OBS, (lower row) EN4.1.1 –
685 OBS. (left) Mean, (Right) RMS. Units are psu. Contours of the RMS variability of
686 0/300m salinity are superposed on upper right panel for comparison (CI = 0.1 psu).
687 Fig. 9 **ts_global_vs_time_compare.pdf** Spatial average of (left) global potential temperature
688 (70°S-60°N) and (right) 40°S-40°N Atlantic salinity anomalies from the 1980-2008
689 climatology in three depth ranges for EN4.1.1 (black), SODA3.4.2 (red), and SODA2.2.4
690 (green). (upper panel) 0-300m, (middle panel) 300-1000m, (lower panel) 1000-2000m.
691 Units are K and psu.
692 Fig. 10 **moc_pdf** Overturning circulation across 26°N in the subtropical North Atlantic. (red)
693 SODA3.4.2, (black) observations. Units are 10^6 m^3/s.
694 Fig. 11 **dp_arctic_profiles.pdf** Time mean stratification 2000-2008 with depth for (black)
695 PHC3.0, SODA3.4.2, and SODA2.2.4 at two locations on opposite sides of the Arctic:

(upper) 84°N, 30°E on the edge of the Nansen Basin near the Atlantic inflow to the Arctic, and (lower) 72.5°N, 150°W in the Canada Basin. Units are °C and psu.

Fig. 12 **arctic_sea_ice_extent.pdf** September Arctic sea ice extent (area with concentration in excess of 15%). Black line indicates observed sea ice extent. Units are 10^{12} m^2.

Fig. 13 **equator_tao_soda342.pdf** Time mean vertical profiles of zonal velocity, potential temperature, and salinity with depth at two longitudes along the Pacific Equator. (Upper) 165°E, (lower) 140°W. Units are: m/s, °C, and psu.

Fig. 14 **97-98_ENSO_342_224.pdf** Monthly average SODA3.4.2 and SODA2.2.4 zonal currents at 5m depth along the Equator Indian and Pacific during the two year period January, 1997 through December, 1998. Units are m/s.

Fig. soda3_data_distrib.pdf
Number of hydrographic profile observations used by SODA3, after spatial and temporal binning to remove redundancies, with depth and time 1980-2015. Upper panel shows temperature, lower panel shows salinity. Units: observations per month.

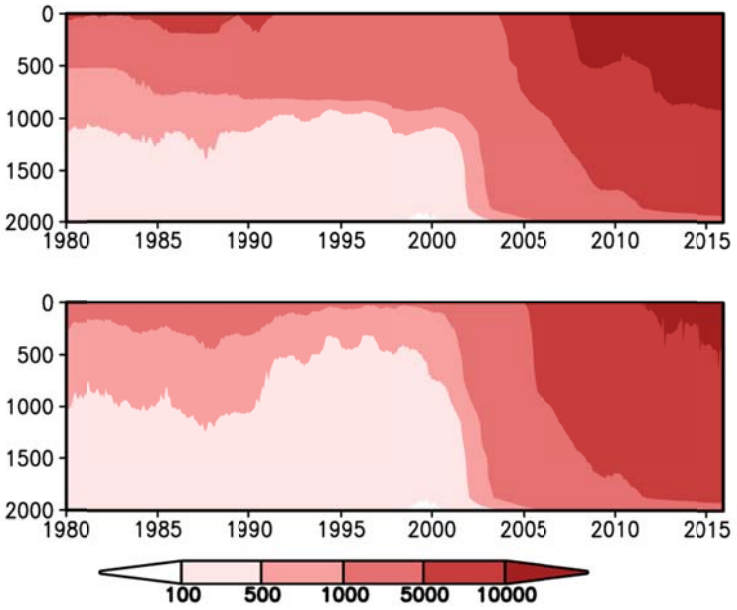

Fig. soda3_global_topography.pdf
ETOP5 topography used in SODA3. Note the inclusion of many marginal seas. Units are m.

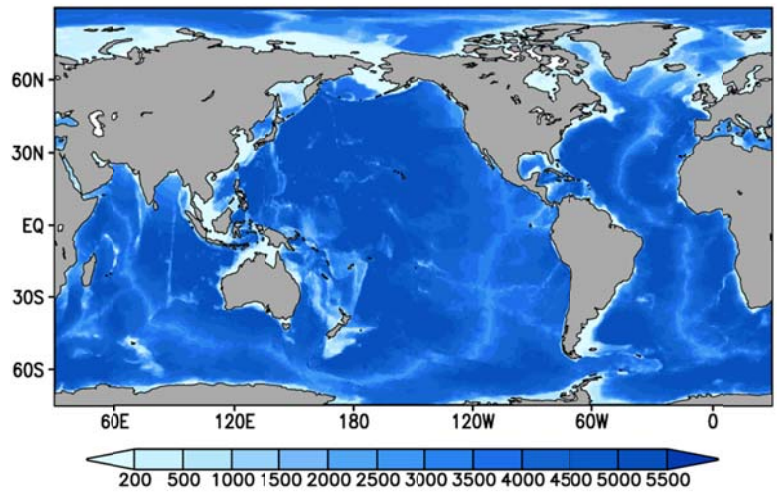

Fig. ts-bermuda.pdf Potential temperature versus salinity for (green) SODA2.2.4, (red) SODA3.4.2, and (black) EN4.1.1 at a fixed location (32°N, 62°W) just east of Bermuda in the subtropical North Atlantic for the nine year period 2000-2008. The temperature/salinity relationship is reasonably consistent among the three except for temperatures below 8°C corresponding to depths below 900m. At those depths SODA2.2.4 shows greater variability. Units are K and psu.

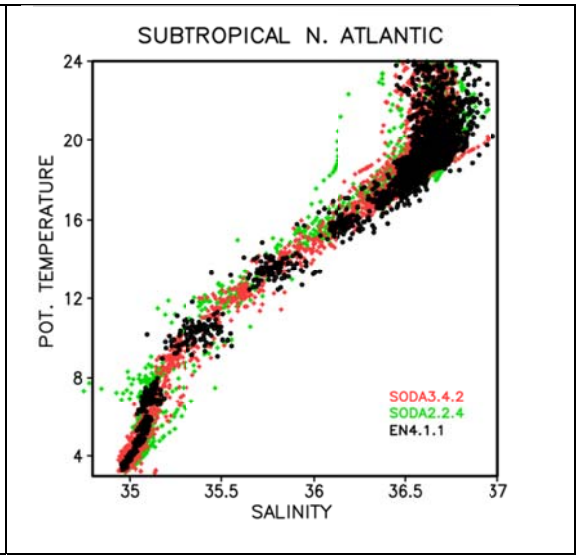

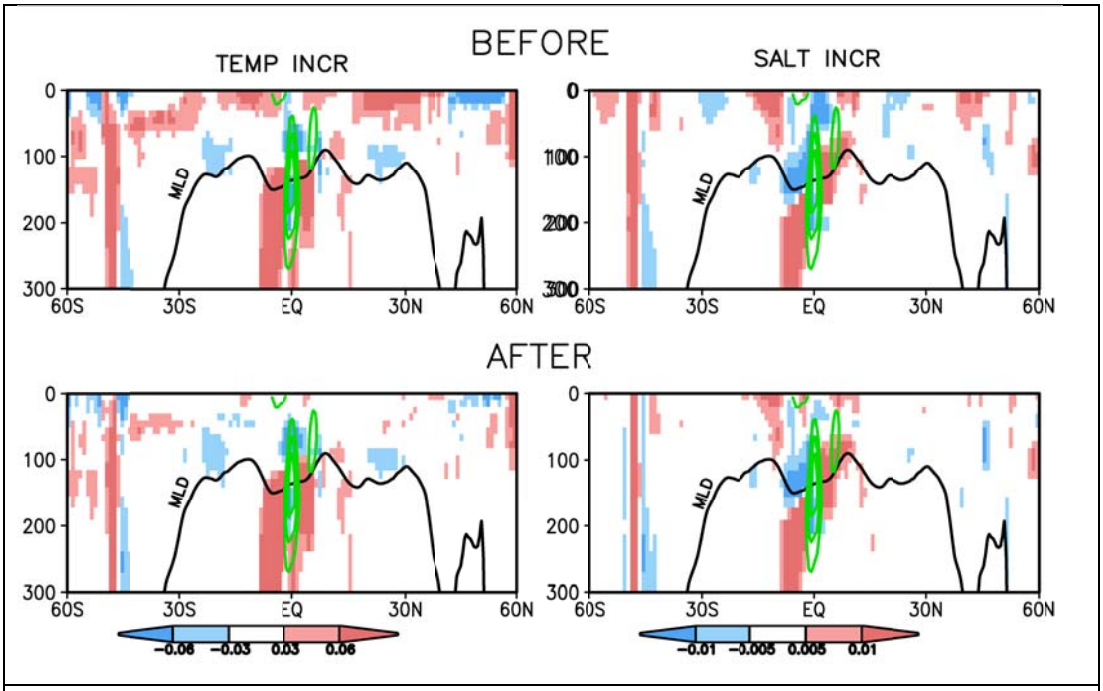

Fig. 180w_increment.pdf Mean (left) temperature increments $\overline{\theta^o - \mathbf{H}(\theta^f)}$ and (right) salinity increments $\overline{S^o - \mathbf{H}(S^f)}$ with latitude and depth, averaged in the longitude band 170°W-180°W for experiments using ERA-Int forcing. The average depth of the density-based mixed layer is shown in black and zonal velocity in green (0.2 m/s contour). Upper panels show analysis increments before heat and freshwater fluxes are corrected. Lower panels show analysis increments

for SODA3.4.2, after heat and freshwater fluxes have been corrected as described in the text. Note the reduction in misfit except near the strong equatorial currents. Units are K/10dy and psu/10dy.

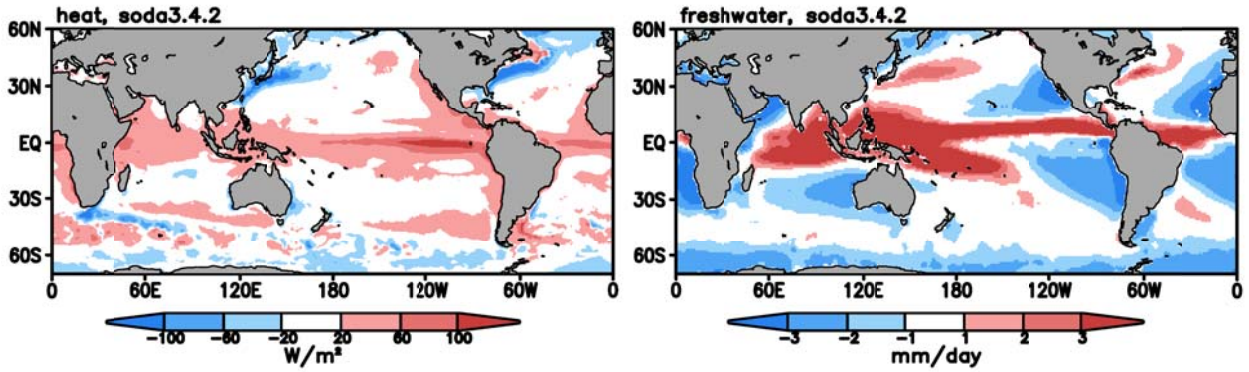

Fig. flxs_soda342.pdf Time mean net surface heat flux for the five reanalysis members. Units are W/m^2 and mm/dy

Fig. SST_compare_342_224.pdf (left) Mean and (right) root mean square difference of monthly SST from the OISST analysis of Reynolds et al. (2007). (upper) SODA3.4.2, (lower) SODA2.2.4. Units are K.

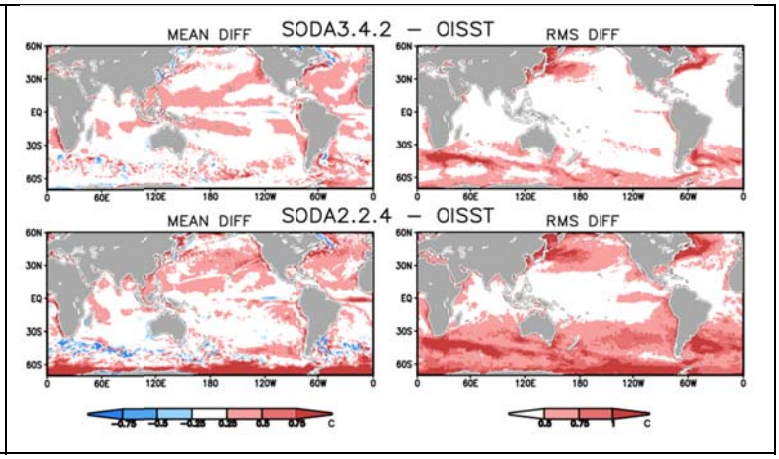

Fig. A-O_temp_comparison.pdf Statistics of the binned analysis minus observation potential temperature differences $\mathbf{H}(\theta^a) - \theta^o$ averaged 0-300m during the 29 year period 1980-2008. (Upper row) SODA3.4.2 - OBS, (middle row) SODA2.2.4 – OBS, (lower row) EN4.1.1 – OBS. (left) Mean, (Right) RMS. Units are K. Contours of the RMS variability of 0/300m temperature are superposed on upper right panel for comparison (CI = 1 K).

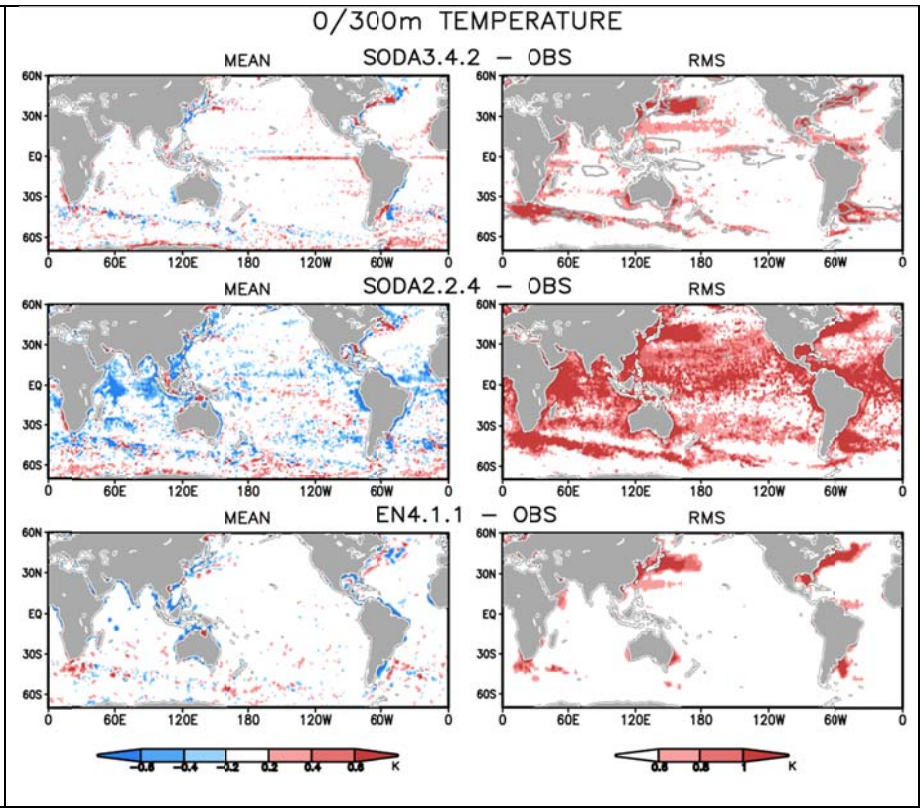

Fig. A-O_salt__comparison.pdf Statistics of the binned analysis minus observation salinity differences $\mathbf{H}(S^a) - S^o$ averaged 0-300m during the 29 year period 1980-2008. (Upper row) SODA3.4.2 - OBS, (middle row) SODA2.2.4 – OBS, (lower row) EN4.1.1 – OBS. (left) Mean, (Right) RMS. Units are psu. Contours of the RMS variability of 0/300m salinity are superposed on upper right panel for comparison (CI = 0.1 psu).

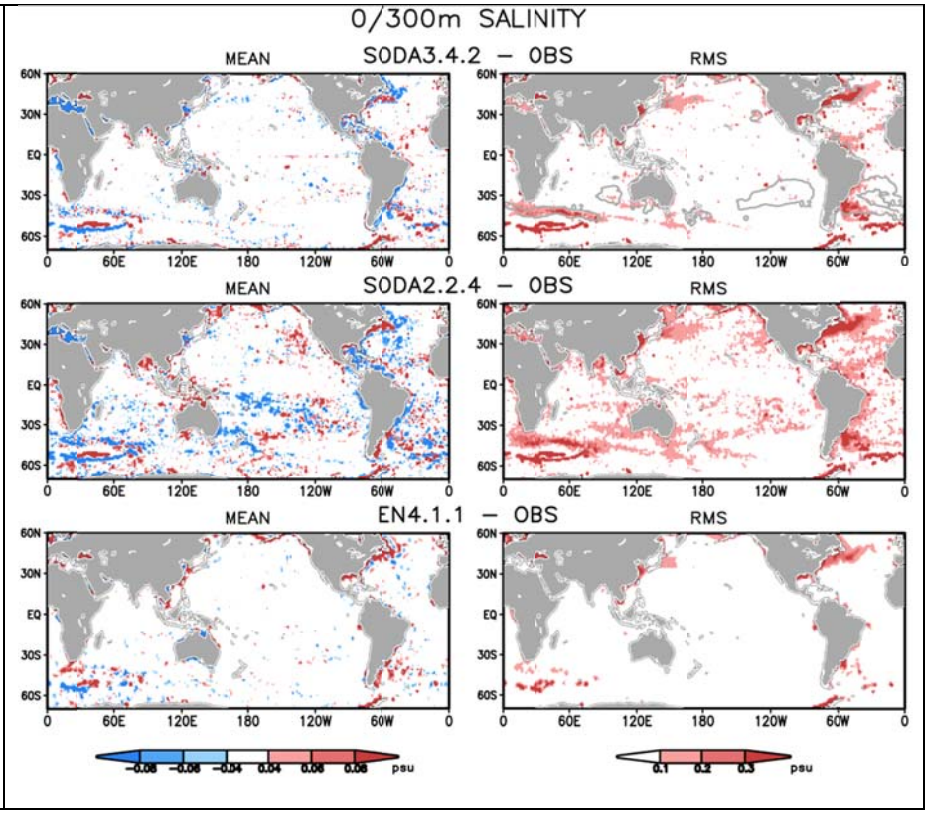

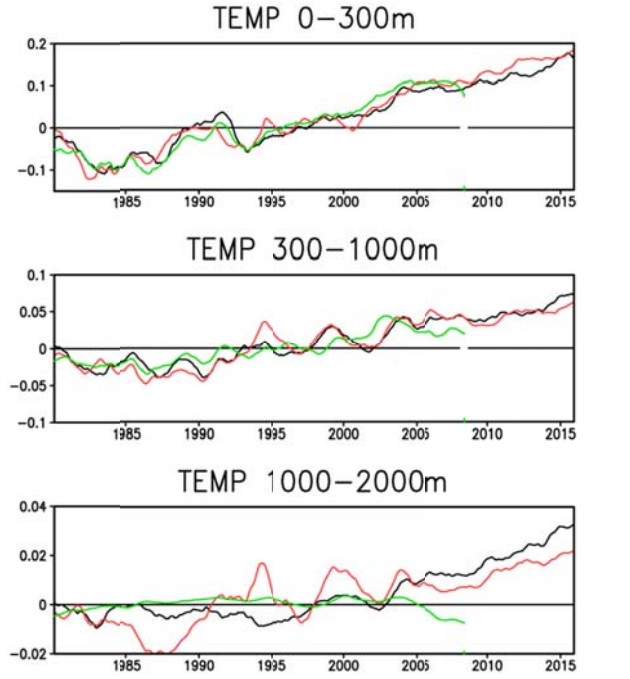

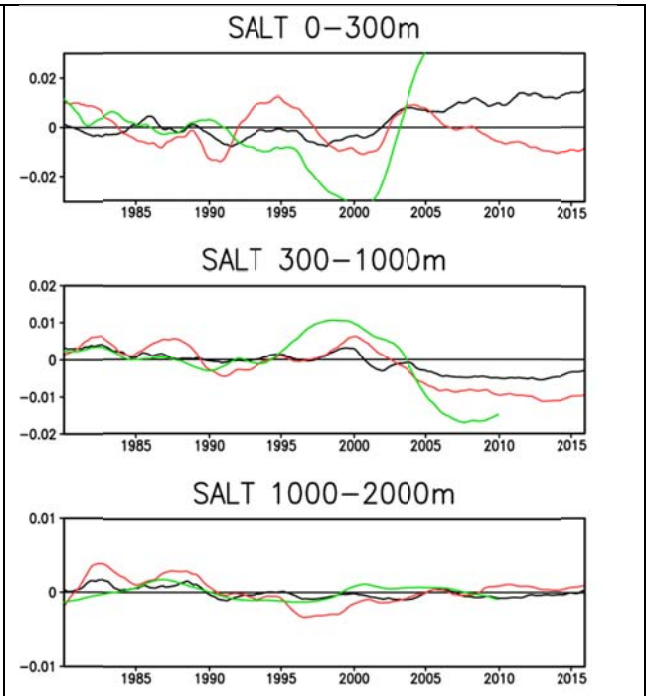

Fig. Tglobal_vs_time_compare.pdf . Sglobal_vs_time_compare.pdf
Spatial average from 70°S-60°N of (left) potential temperature and (right) salinity anomalies from their monthly climatology in different depth ranges for the EN4.1.1 objective analysis (black), SODA3.4.2 (red), and SODA2.2.4 (green). (upper panel) 0-300m, (middle panel) 300-1000m, (lower panel) 1000-2000m. Units are K and psu. ADD Pinatubo. Label lines. Combine into a single fig.

Fig. Satlantic_vs_time_compare.pdf
Salinity anomalies in the Atlantic versus time averaged 50°S-50° and with depth 0-300m. EN4.1.1 objective analysis (black), SODA3.4.2 (red), and SODA2.2.4 (green). Time series has been smoothed with a running 4-year smooth. The time when the ARGO system expanded is indicated.

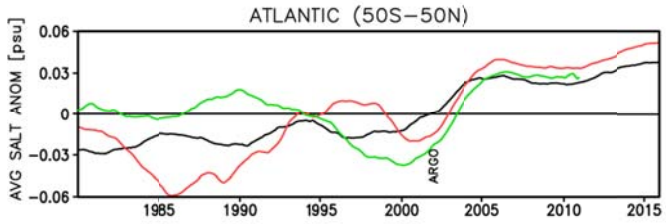

Fig. dp_arctic_profiles.pdf Time mean stratification 2000-2008 with depth for (black) PHC3.0, SODA3.4.2, and SODA2.2.4 at two locations on opposite sides of the Arctic: (upper) 84°N, 30°E on the edge of the Nansen Basin near the Atlantic inflow to the Arctic, and (lower) 80°N, 150°W in the Canada Basin. Units are °C and psu..

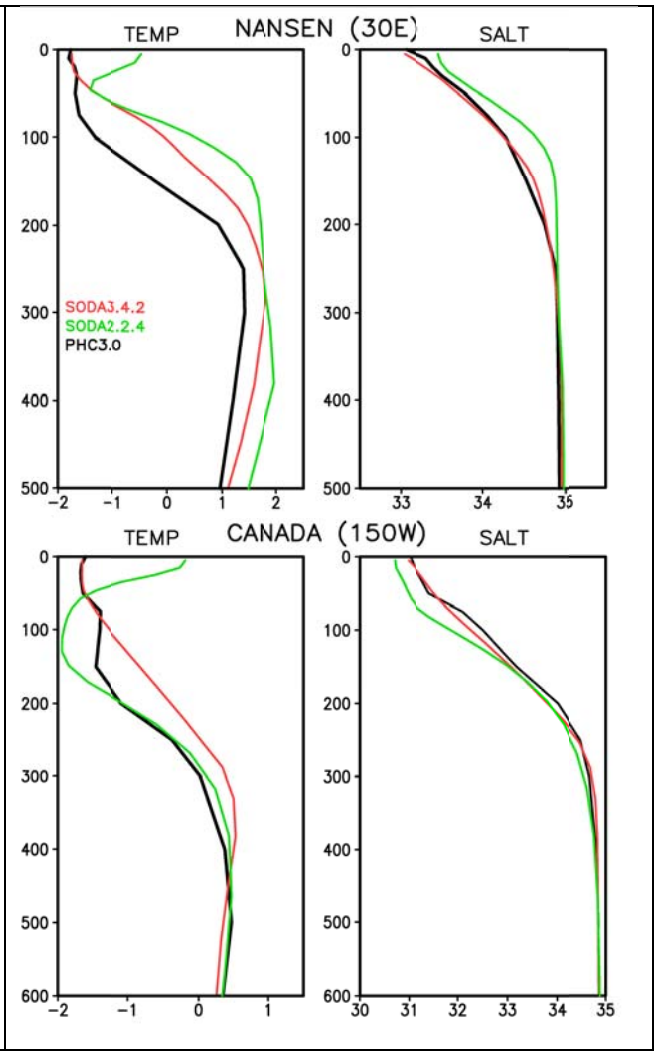

Fig. arctic_sea_ice_extent.pdf September Arctic sea ice extent (area with concentration in excess of 15%). Black line indicates observed sea ice extent. Units are 10^{12} m^2.

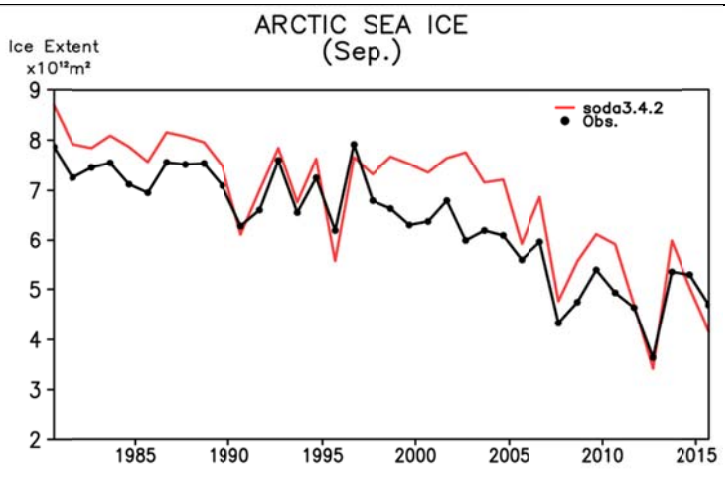

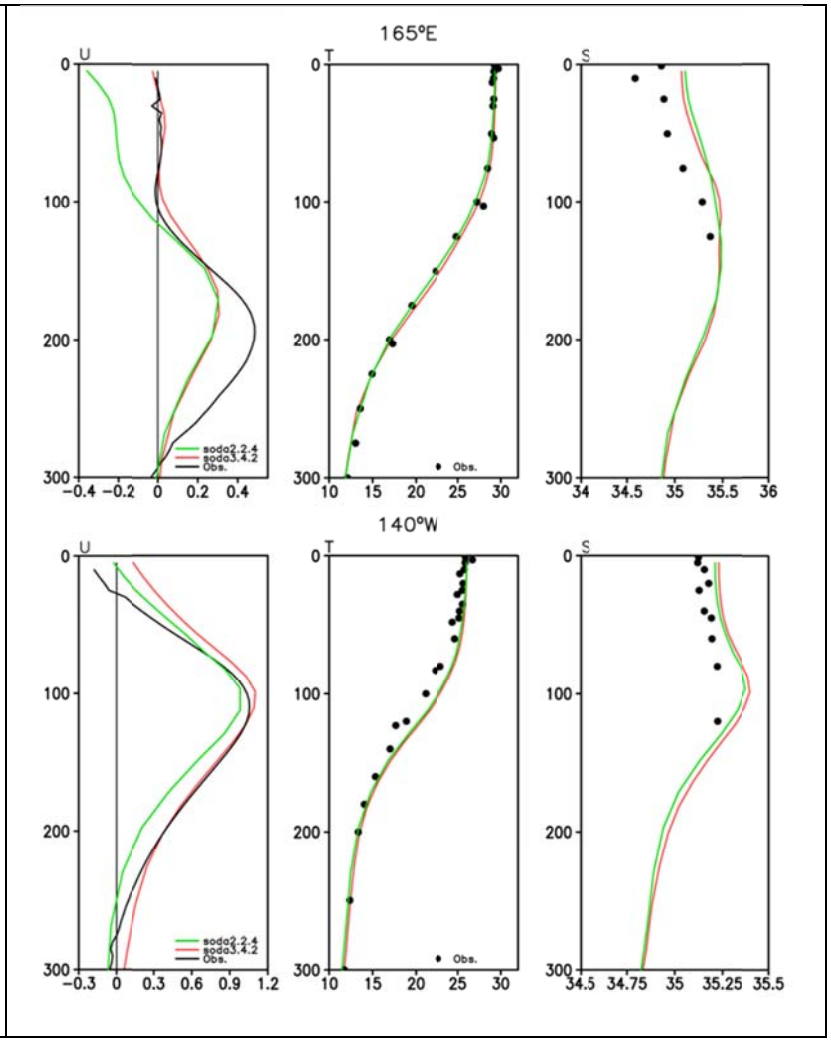

Fig. equator_equator_tao_2.pdf Time mean vertical profiles of zonal velocity, potential temperature, and salinity with depth for the five experiments shown in **Table 2** at two longitudes along the Pacific Equator. (Upper) 165°E, (lower) 140°W. Observations are shown in black. Units are: m/s, °C, and psu.

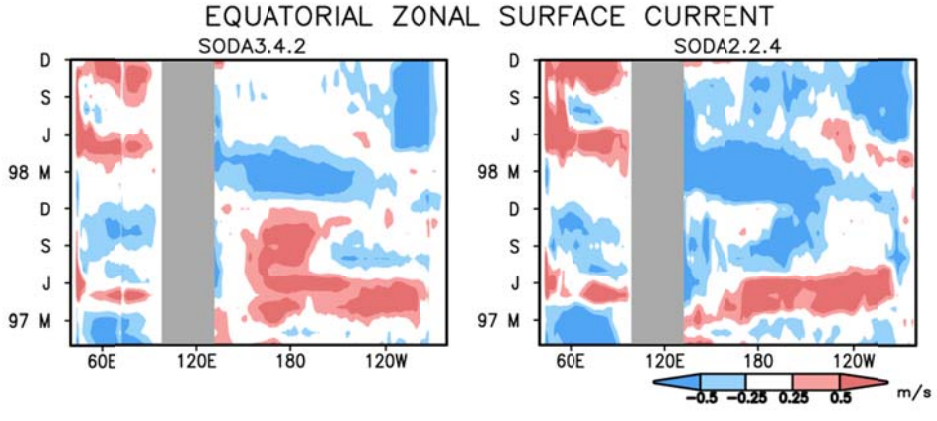

Fig. 97-98_ENSO_342_224.pdf Monthly average SODA3.4.2 and

SODA2.2.4 zonal currents at 5m depth along the Equator Indian and Pacific during the two year period January, 1997 through December, 1998. Units are m/s.

Supplemental Material for:

SODA3: a new ocean climate reanalysis

James A. Carton, Gennady A. Chepurin, and Ligang Chen

Introduction

Here we provide additional figures and discussion to highlight three issues raised in the main text of Carton et al. (2018): the switch of SST data sources in 2002, the changes to the topography data set when moving from SODA2 to SODA3, and the modification of seasonal ERA-Interim heat and freshwater fluxes based on an iterative procedure that involves carrying out a preliminary reanalysis experiment to identify the seasonal mixed layer temperature and salinity analysis increments.

SST Data: In 2002 we switch from Pathfinder v5.2 L3 satellite infrared SST, which finishes in 2013, to ACSPO which begins in 2002 and includes additional satellite data sets. We make the switch in 2002 for two reasons. First, we found a cooling trend in Pathfinder SST that does not occur in either ACSPO or in the gridded OISSSTv2 product (**Fig. S1** lower panel). This trend lowers global Pathfinder SST by ~0.25°C (even more in the Pacific warm pool). Another reason to switch is that Pathfinder SST measures skin temperature and must be corrected to be appropriate for the depth of the first model level (bulk SST). ACSPO does not require this additional correction (**Fig. S1** upper panels).

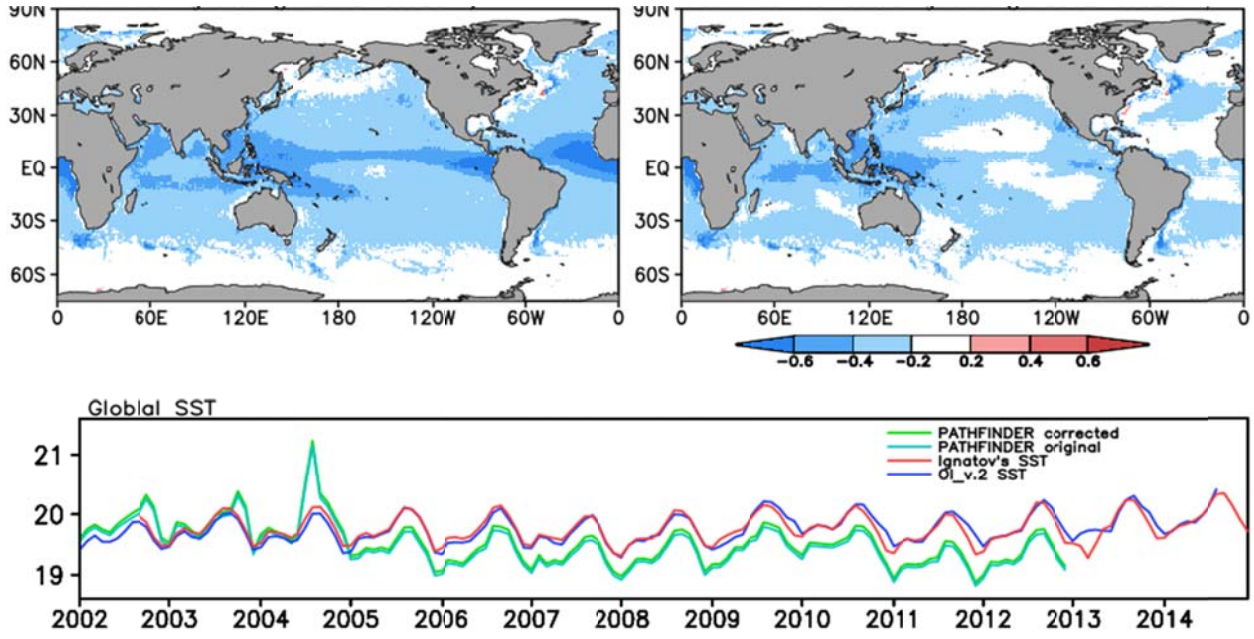

Fig. S1 Comparison of Pathfinder v5.2 L3 SST and the ACSPO L3 bulk SST of Ignatov et al. (2016) for the 12 year period 2002-2013. (Upper left) time mean difference between Pathfinder and ACSPO, (upper right) reduced time mean difference between Pathfinder SST corrected to bulk SST following Grodsky et al. (2008) and ACSPO SST. (lower) Global average monthly Pathfinder SST, ACSPO SST, and OISSTv2 2002-2015. Pathfinder SST is only available until 2014.

Topography SODA3 uses a somewhat finer topography data set that improves resolution of key passages. In **Fig. S2** we show a detailed view of the topography of the passages connecting the Pacific and Indian Oceans where the impact of the change in resolution is evident.

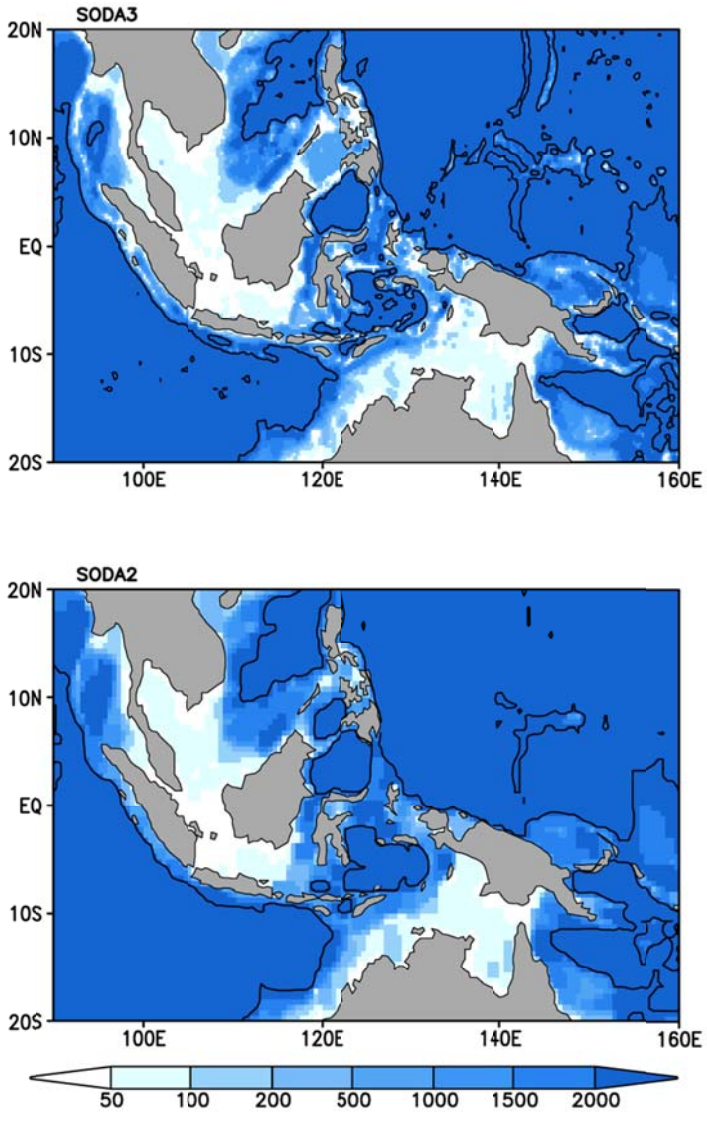

Fig. S2 Comparison of the topography of the tropical western Pacific/eastern Indian Ocean as it appears in (upper) SODA3 and (lower) SODA2. The 2500m contour is included. Note the improved resolution in SODA3. Units are: m.

Fluxes: In the main text we point out that surface heat and freshwater fluxes calculated directly from ERA-Interim surface variables are incompatible with the ocean observation set. This incompatibility is indicated by the existence of systematic (e.g. time mean) analysis increments of temperature and salinity within the mixed layer. We apply the methodology of Carton et al. (2018) to construct seasonal modifications of ERA-Interim net surface heat and freshwater flux of which the time mean is shown in **Fig. S3**. Among the striking changes we impose: time mean net surface heat flux in the subtropical gyres is increased by 10-30W/m^2 while net evaporation is

increased by 1-3 mm/dy. In contrast, rain over the west Pacific warm pool in increased by 1 mm/dy.

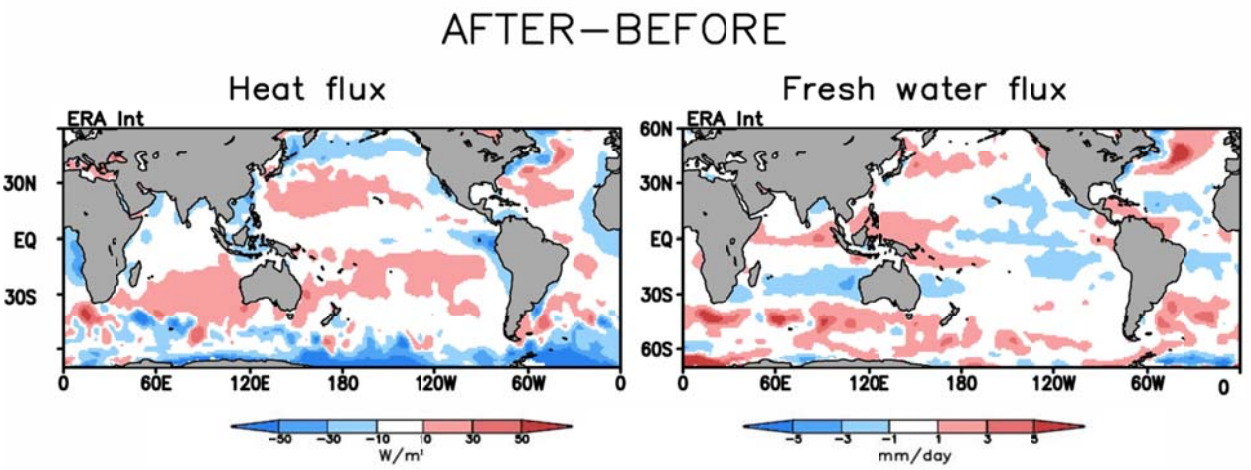

Fig. S3 Time mean modifications to net surface heat and freshwater flux obtained through application of (1.3) to an initial reanalysis experiment. Units are: W/m^2 and mm/dy.